Zhang, W. and Chen, Q. 2000. "Large eddy simulation of natural and mixed convection airflow indoors with two simple filtered dynamic subgrid scale models." *Numerical Heat Transfer, Part A: Applications*, 37(5), 447-463.

LARGE EDDY SIMULATION OF NATURAL AND MIXED CONVECTION AIRFLOW INDOORS WITH TWO SIMPLE FILTERED DYNAMIC SUBGRID SCALE MODELS

Wei Zhang and Qingyan Chen
Building Technology Program
Massachusetts Institute of Technology
77 Mass. Ave., Cambridge, MA 02139-4307, USA
Phone: (617) 253-7714, fax: (617) 253-6152, email: qchen@mit.edu

ABSTRACT

Large eddy simulation (LES) with a dynamic subgrid-scale model (DSM) is a powerful tool to predict indoor airflow. Some DSM models need to average the model coefficient over a homogeneous direction or need to use an additional parameter. The others are too complicated. This study proposes a simple filtered dynamic subgrid scale model (FDSM) for indoor flow without a homogeneous direction. The predicted air velocity, air temperature and turbulence distributions agree reasonably well with the experimental data. The results show that the FDSM can be used to simulate indoor airflow.

NOMENCLATURE

Ar :	Archimedes number
C:	Model coefficient ($C=Cs^2$)
Cs:	Smagorinsky model coefficient
D:	Room depth
$G(x_i)$:	Filter function
g:	Gravitational acceleration
H:	Room height
L:	Room width
$\overline{p}_i$:	Grid filtered pressure
Pr:	Molecular prandtl number
Pr_{SGS}:	Subgrid-scale prandtl number
Ra:	Rayleigh number
T:	Temperature
u_i :	Velocities
$\overline{u}_i$:	Grid filtered velocities
$\widetilde{\overline{u}}_i$:	Test filtered velocities
T:	Tempearture
x_i :	Cartesian space coordinate

Greek symbols

β :	Thermal expansion coefficient
Δt :	Time step
Δ :	Filter size
ν :	Kinematic viscocity
$\overline{\theta}$:	Grid filtered temperature
$\widetilde{\overline{\theta}}$:	Test filtered temperature

INTRODUCTION

To design a comfortable and healthy indoor environment, one requires information about the distributions of air velocity, air temperature, relative humidity, contaminant concentrations, and turbulent quantities in the indoor environment. This information can be obtained numerically by using a computational fluid dynamics (CFD) program with a Reynolds averaged Navier-Stokes equation model. However, the power spectrum of the airflow may play an important role in the thermal comfort. A CFD program with a Reynolds averaged Navier-Stokes equation model cannot predict the power spectrum. However, with a large eddy simulation (LES) model, a CFD program can calculate the power spectrum. A CFD program with a LES model should be a next-generation tool to study indoor airflow, because the model is more universal, has fewer or no adjustable model coefficients, and can provide more flow information than other CFD models.

Typical indoor airflow includes natural convection, such as winter heating by a baseboard heater; forced convection, such as free cooling in shoulder seasons; and mixed convection, such as summer cooling with an air conditioner. The indoor airflow is complex and is driven by pressure gradients and thermal buoyancy.

Very few LES studies on indoor airflow have been reported [3, 4, 10]. The results in these studies does not agree very well with the experimental data. This is probably due to a constant model coefficient used in the Smagorinsky model [13]. The Smagorinsky model has some notable drawbacks including: (a) the requirement of a model coefficient C that is flow dependent; (b) incorrect prediction of the asymptotic behavior near a wall; and (c) no permission of SGS (Sub-grid scale) energy backscatter to the resolved scales.

On the other hand, Germano et al. [5] and Lilly [8] proposed a dynamic subgrid scale model (DSM) to solve the problems associated with the Smagorinsky model by directly computing directly the model coefficient with the information from the resolved scales. This model can also correctly predict the asymptotic behavior near a wall, and permits energy backscatter from small to large scales. However, DSM requires averaging the coefficient over a homogeneous flow direction (statistical homogeneity) because the coefficient fluctuates significantly. The averaging procedure can dampen large fluctuations of the C often encountered in a flow prediction. This procedure gives good results for simple flows with at least one homogeneous direction, such as a turbulent channel flow. However, it cannot be used for a flow without a homogeneous direction.

Recently, Ghosal et al. [6] proposed a fully localized model based on a constrained variation approach. This approach solves Fredholm's integral equation of a second kind and is very complicated. Since the model is not developed for indoor airflow, the performance of this model for complex indoor airflow is unknown.

Another approach by Meneveau et al. [9] used a Lagrangian dynamic model. This model is suitable for inhomogeneous flows and the results look encouraging. The model needs an additional parameter, the Lagrangian averaging time, which needs to be prescribed. Additional tests are required to establish how to calculate this parameter [11].

Most indoor airflows do not have a homogeneous direction, and the available approaches seem too complicated for indoor airflow. Therefore, it is necessary to find a simple method to determine the DSM coefficient for an inhomogeneous indoor airflow. This investigation proposes a filtered dynamic subgrid scale model (FDSM) that uses the filter technique to determine the model coefficient for indoor airflow without a homogeneous direction.

THE FILTERED DYNAMIC SUBGRID-SCALE MODEL (FDSM)

Filter Function and Filtered Navier-Stokes Equations

The LES requires the separation of small-eddies from large-eddies with a filter. For simplicity, the following section uses a one-dimensional notation. The filtered velocity is

$$\overline{u_i} = \int G(x, x')u_i(x)dx' \tag{1}$$

where G(x, x') is a filter function. The filter function is large only when G (x, x') is less than the filter width, a length scale over which averaging is performed. The flow eddies larger than the filter width are "large-eddies," and those smaller than the width are "small-eddies".

This paper uses a box filter, i.e.

$$G(x_i) = \begin{cases} \dfrac{1}{\Delta_i} & (|x_i| \le \dfrac{\Delta_i}{2}) \\ 0 & (|x_i| > \dfrac{\Delta_i}{2}) \end{cases}, \tag{2}$$

With the finite volume method, it seems natural to define the filter width, $\Delta_i = (\Delta x_1 \Delta x_2 \Delta x_3)^{\frac{1}{3}}$, as an average over a grid volume.

With the filter, it is possible to derive the governing conservation equations for the momentum (Navier-Stokes equations), mass continuity, and energy. The filtered Navier-Stokes equations for an incompressible flow are

$$\frac{\partial \overline{u_i}}{\partial t} + \frac{\partial}{\partial x_j}(\overline{u_i} \cdot \overline{u_j}) = -\frac{1}{\rho}\frac{\partial \overline{P}}{\partial x_i} + \upsilon \frac{\partial^2 \overline{u_i}}{\partial x_i \partial x_j} - \frac{\partial \tau_{ij}}{\partial x_j} + g_j \beta(\overline{\theta} - \theta_0)\delta_{ij} \tag{3}$$

where the subgrid Reynolds stresses are

$$\tau_{ij} = \overline{u_i u_j} - \overline{u_i} \cdot \overline{u_j} \tag{4}$$

LES also solves the filtered energy equation with subgrid heat flux terms for flow problems with heat transfer

$$\frac{\partial \overline{\theta}}{\partial t} + \frac{\partial \overline{u}_j \overline{\theta}}{\partial x_j} = \frac{\partial}{\partial x_j}\left(\frac{\upsilon}{Pr}\frac{\partial \overline{\theta}}{\partial x_j}\right) - \frac{\partial h_j}{\partial x_j} \tag{5}$$

where the sugrid heat fluxes are

$$h_j = \overline{u_j \theta} - \overline{u}_j \overline{\theta} \tag{6}$$

The terms in the above equations, $\overline{u_i u_j}$ and $\overline{u_j \theta}$, are unknown and need to be modeled.

The Filtered Dynamic Subgrid Scale Model Coefficient

Smagorinsky model In order to close the equations, the subgrid Reynolds stresses and heat fluxes can be modeled using the Smagorinsky model and the simplified Boussinesq approximation.

$$\tau_{ij} = 2C_\tau \overline{\Delta}^2 |\overline{S}| \overline{S}_{ij} \tag{7}$$

$$h_j = \frac{1}{Pr_{SGS}} C_\tau \overline{\Delta}^2 |\overline{S}| \frac{\partial \overline{\theta}}{\partial x_j} \tag{8}$$

where, $|\overline{S}| = (2\overline{S_{ij}} \cdot \overline{S_{ij}})^{\frac{1}{2}}$, $\overline{S_{ij}} = \frac{1}{2}\left(\frac{\partial \overline{u_i}}{\partial x_j} + \frac{\partial \overline{u_j}}{\partial x_i}\right)$, $C\tau = Cs^2$, $Cs = 0.1 \sim 0.25$, and $Pr_{SGS} = 0.5$

However, the Smagorinsky model coefficient C is flow dependent.

Dynamic sub-grid scale model (DSM) On the other hand, the DSM [5] calculates the model coefficient by relating the subgrid scale Reynolds stresses to two different sizes of filters. Since the Reynolds stresses vary with time and location, the resulting model coefficient is therefore a function of time and location.

The DSM uses an explicit test filter, $\widetilde{G}$, with a filter width of $\widetilde{\Delta}$ ($\widetilde{\Delta} = 2\overline{\Delta}$) [5] to determine the turbulent stresses on the test filter ($\widetilde{G}$ filter)

$$T_{ij} = \overline{\widetilde{u_i u_j}} - \widetilde{\overline{u}}_i \widetilde{\overline{u}}_j \tag{9}$$

The first term on the right side of Eq. (9) cannot be determined directly, like the one in Eq. (4). However, substituting Eq. (9) from the Eq. (4) with a test filter can eliminate the terms

$$T_{ij} - \widetilde{\tau}_{ij} = L_{ij} \tag{10}$$

where, $L_{ij} = \widetilde{\overline{u}_i \overline{u}_j} - \widetilde{\overline{u}}_i \widetilde{\overline{u}}_j$

The resolved turbulent stresses, L_{ij}, in Eq. (10) can be calculated explicitly. With the definition of the Smagorinsky model, the DSM coefficient C can be determined. By using the same procedure, the dynamic subgrid scale turbulent Prandtl number can also be obtained [8]. More detailed information about the DSM can be found in [5] and [8].

Filtered dynamic sub-grid scale model (FDSM) Note that all of the terms in Eq. (10) are related to the test filter ($\widetilde{\Delta}$). The model coefficient C obtained with Eq. (10) should be valid for the test filter ($\widetilde{\Delta}$). Since the subgrid scale Reynolds stresses, τ_{ij}, are defined with the grid filter ($\overline{\Delta}$), the model coefficient C should be related to the grid filter ($\overline{\Delta}$). This can be done by applying a grid filter to Eq. (10) to yield

$$\overline{T}_{ij} - \widetilde{\overline{\tau}}_{ij} = \overline{L}_{ij} \tag{11}$$

In order to obtain a new model coefficient from Eq. (11), the τ_{ij} and the T_{ij} in Eq. (11) are modeled by using the Smagorinsky model or the mixed model [15] . However, this modeling would lead to an error in satisfying Eq. (11), τ_{ij}^{model}.

$$e_{ij} = \overline{L}_{ij} - (\overline{T}_{ij}^{model} - \widetilde{\overline{\tau}}_{ij}^{model}) \tag{12}$$

For simplicity, this investigation used the Smagorinsky model for modeling. The corresponding error is

$$e_{ij} = \overline{L}_{ij} - \overline{2C_T \widetilde{\overline{\Delta}}^2 \left|\widetilde{\overline{S}}\right| \widetilde{\overline{S}}_{ij}} + \overline{2C_\tau \overline{\Delta}^2 |\overline{S}| \overline{S}_{ij}} \tag{13}$$

Using the definitions of $\alpha_{ij} = 2\widetilde{\overline{\Delta}}^2 \left|\widetilde{\overline{S}}\right| \widetilde{\overline{S}}_{ij}$ and $\beta_{ij} = 2\overline{\Delta}^2 |\overline{S}| \overline{S}_{ij}$, Eq. (13) can be rewritten as

$$e_{ij} = \overline{L}_{ij} - \overline{C_T \alpha_{ij}} + \overline{C_\tau \beta_{ij}} \tag{14}$$

If we assume

$$\overline{C_T \alpha_{ij}} \approx \overline{C}_T \overline{\alpha}_{ij}, \tag{15}$$

$$\overline{C_\tau \beta_{ij}} \approx \widetilde{\overline{C}}_\tau \widetilde{\overline{\beta}}_{ij} \tag{16}$$

$$C \approx \widetilde{\overline{C}}_\tau \approx \overline{C}_T . \tag{17}$$

then Eq. (13) becomes

$$e_{ij} = \overline{L}_{ij} - \overline{C_T \alpha_{ij}} + \overline{C_\tau \beta_{ij}} = \overline{L}_{ij} - C\overline{M}_{ij} \tag{18}$$

where $M_{ij} = \alpha_{ij} - \widetilde{\beta}_{ij}$

Meneveau et al. [9] used direct numerical simulation (DNS) data to analyze the two hypotheses used in the DSM. They filtered DNS data at both a grid filter and a test filter, and then they compared the coefficients obtained with and without the time averaging procedure. Although the two coefficients are not equal without averaging, they are similar with the time averaging:

$$C^{DNS}{}_\tau \neq C^{DNS}{}_T \tag{19}$$

$$\{C^{DNS}{}_\tau\} \approx \{C^{DNS}{}_T\} \tag{20}$$

where $\{\}$ denotes the time averaging. Meneveau et al. [9] also discussed the minimal error caused by approximating $\widetilde{C_\tau \beta_{ij}} = \widetilde{C}_\tau \widetilde{\beta}_{ij}$ with and without using the averaging technique. The study shows that the minimal error with the averaging is much smaller than that without the averaging:

$$\text{Error}_{\min}(\{\widetilde{C}_\tau \widetilde{\beta}_{ij}\}, \{\widetilde{C_\tau \beta_{ij}}\}) << \text{Error}_{\min}(\widetilde{C}_\tau \widetilde{\beta}_{ij}, \widetilde{C_\tau \beta_{ij}}) \tag{21}$$

Since the filtering technique is averaging, the results obtained by Meneveau et al. (1996) may be extended to the grid filtering technique. Therefore, the assumptions used in Eqs. (15), (16), and (17) may be valid as well, although they still need to be examined further.

The present investigation uses the least-square approach to obtain the model coefficient, the C in Eq. (18), as suggested by Lilly [8] and Ghosal et al. [6]. At any given point in a space, $\mathbf{x}$, the e_{ij} is a function of the C. In order to obtain an optimal C, the e_{ij} should be integrated over the entire flow domain with a smooth function, because the square of the residual, $e_{ij}e_{ij}$, may have locally violent changes. The integrated square of the error function, $E_{ij}(C)$, is

$$E_{ij}(C) = \int G_f(\mathbf{x},\mathbf{x}')\, e_{ij}(\mathbf{x}')\, e_{ij}(\mathbf{x}')\, d\mathbf{x}' \tag{22}$$

where $G_f(\mathbf{x},\mathbf{x}')$ is a smooth function. Substitute Eq. (18) into Eq.(22), and Eq. (22) reads:

$$E_{ij}(C) = \int G_f(\mathbf{x},\mathbf{x}')(\overline{L}_{ij} - C\overline{M}_{ij})^2\, d\mathbf{x}' \tag{23}$$

Since the least square condition for the Eq. (23) is $\frac{\partial E_{ij}(C)}{\partial C} = 0$, then the optimal model coefficient C is obtained as:

$$C = \frac{\int G_f(\mathbf{x},\mathbf{x}')\, \overline{L}_{ij} \overline{M}_{ij}\, d\mathbf{x}'}{\int G_f(\mathbf{x},\mathbf{x}')\, \overline{M}_{ij} \overline{M}_{ij}\, d\mathbf{x}'} \tag{24}$$

The C is obviously a function of time and space, and it can be applied to inhomogeneous flows. The smooth function $G_f(\mathbf{x},\mathbf{x}')$ should be chosen for the entire flow domain and may depend on the turbulent scales. Although the smooth function can be in many forms, a box filter (Eq. (2)) may be the most convenient ($G_f(\mathbf{x},\mathbf{x}') = G(\mathbf{x},\mathbf{x}')$). The filter can be either a grid filter or a test filter

$$C = \frac{\overline{\overline{L}_{ij} \overline{M}_{ij}}}{\overline{\overline{M}_{ij} \overline{M}_{ij}}} \quad \text{(with the grid filter } \overline{\Delta}\text{)} \tag{25}$$

or

$$C = \frac{\overline{L_{ij}}\,\widetilde{\overline{M}_{ij}}}{\widetilde{\overline{M}_{ij}}\,\overline{M}_{ij}} \quad \text{(with the test filter } \widetilde{\overline{\Delta}}\text{)} \tag{26}$$

Eqs. (25) and (26) are now defined as the filtered dynamic subgrid scale model (FDSM). The $FDSM_G$ has the grid filter in Eq. (25), and $FDSM_T$ has the test filter in Eq. (26). The function of the grid filter is to average the coefficient and to smooth the large fluctuation of the coefficient. The filter technique will lead to a stable numerical solution. The FDSM can be considered as a simple model compared with those proposed by Ghosal et al. [6] and Meneveau et al. [9].

The $FDSM_G$ or $FDSM_T$ can also be locally negative. According to Piomelli et al. [12], a negative C indicates a negative eddy viscosity and implies an energy transfer from small scales to the resolved scales or backscatter. However, the negative C can also lead to a numerical instability. In order to avoid the instability, the present investigation uses C = Max (0.0, Eq.(25) or (26)) that is also used by the others [10].

Filtered dynamic subgrid turbulent Prandtl number Similarly, we can also calculate the Prandtl number in the dynamic subgrid heat fluxes with the same procedure. The subgrid heat flux on the test filter ($\widetilde{G}$ filter) is

$$H_j = \widetilde{\overline{u_j \theta}} - \widetilde{\overline{u}}_j \widetilde{\overline{\theta}} \tag{27}$$

Substitute Eq. (27) from the Eq. (6) with a test filter

$$H_j - \widetilde{h}_j = R_j \tag{28}$$

where $R_j = \widetilde{\overline{u}_j \overline{\theta}} - \widetilde{\overline{u}}_j \widetilde{\overline{\theta}}$ and apply a grid filter to Eq. (28). Then the equation becomes

$$\overline{H}_j - \widetilde{\overline{h}}_j = \overline{R}_j \tag{29}$$

Now all the terms in Eq. (29) are related to the grid filter. If h_j and H_j in Eq. (29) are replaced by a simplified Boussinesq approximation, the replacement leads to an error in satisfying Eq. (29). The error associated with a model, h_j^{model}, is given by

$$e^h{}_j = \overline{R}_j - (\overline{H}_j^{model} - \widetilde{\overline{h}}_j^{model}) \tag{30}$$

With the simplified Boussinesq approximation,

$$h_j = 2C_\tau \overline{\Delta}^2 \frac{|\overline{S}|}{Pr^h{}_{SGS}} \frac{\partial \overline{\theta}}{\partial x_j}, \text{ and } H_j = 2C_T \widetilde{\overline{\Delta}}^2 \frac{\left|\widetilde{\overline{S}}\right|}{Pr^H{}_{SGS}} \frac{\partial \widetilde{\overline{\theta}}}{\partial x_j} \tag{31}$$

If we define $\alpha^H{}_j = 2\widetilde{\overline{\Delta}}^2 \left|\widetilde{\overline{S}}\right| \frac{\partial \widetilde{\overline{\theta}}}{\partial x_j}$ and $\beta^h{}_j = 2\overline{\Delta}^2 |\overline{S}| \frac{\partial \overline{\theta}}{\partial x_j}$, then Eq. (30) can be rewritten as

$$e_j^h = \overline{R}_j - (\overline{C_T \frac{1}{Pr_{SGS}^H} \alpha^H{}_j} - \widetilde{\overline{C_\tau \frac{1}{Pr_{SGS}^h} \beta^h{}_j}}) \approx \overline{R}_j - C(\overline{\frac{1}{Pr_{SGS}^H} \alpha^H{}_j} - \widetilde{\overline{\frac{1}{Pr_{SGS}^h} \beta^h{}_j}}) \tag{32}$$

With the following assumptions

$$\overline{\alpha^H{}_j \frac{1}{Pr_{SGS}^H}} \approx \overline{\alpha}^H{}_j \overline{\frac{1}{Pr_{SGS}^H}} \tag{33}$$

$$\overline{\beta_j^h \frac{1}{Pr_{SGS}^h}} \approx \overline{\tilde{\beta}_j^h} \overline{\frac{1}{Pr_{SGS}^h}} \tag{34}$$

$$\overline{\frac{1}{Pr_{SGS}^h}} \approx \overline{\frac{1}{Pr_{SGS}^H}} \approx \frac{1}{Pr_{SGS}} \tag{35}$$

Eq. (32) becomes,

$$e_j^h = \overline{R}_j - C\frac{1}{Pr_{SGS}}\tilde{\overline{P}}_j \tag{36}$$

where $P_j = \alpha_j^H - \beta_j^h$.

By using the least-square approach, we also can obtain an optimal $\frac{1}{Pr_{SGS}}$. The integrated square of the error function, $E_j^h(\frac{1}{Pr_{SGS}})$, is

$$E^h{}_j(\frac{1}{Pr_{SGS}}) = \int G_f^h(\mathbf{x},\mathbf{x}')\, e^h{}_j(\mathbf{x}')\, e^h{}_j(\mathbf{x}')\, d\mathbf{x}' \tag{37}$$

where $G_f^h(\mathbf{x},\mathbf{x}')$ is a smooth function.

Substitute Eq. (36) into Eq.(37)

$$E^h{}_j(\frac{1}{Pr_{SGS}}) = \int G_f^h(\mathbf{x},\mathbf{x}')(\overline{R}_j - C\frac{1}{Pr_{SGS}}\overline{P}_j)^2\, d\mathbf{x}' \tag{38}$$

Since the least square condition for the Eq.(38) is $\frac{\partial E_j^h(\frac{1}{Pr_{SGS}})}{\partial(\frac{1}{Pr_{SGS}})} = 0$, then the optimal subgrid turbulent Prandtl number $\frac{1}{Pr_{SGS}}$ is obtained as:

$$\frac{1}{Pr_{SGS}} = \frac{1}{C}\frac{\int G_f^h(\mathbf{x},\mathbf{x}')\,\overline{R}_j\overline{P}_j d\mathbf{x}'}{\int G_f^h(\mathbf{x},\mathbf{x}')\,\overline{P}_j\overline{P}_j d\mathbf{x}'} \tag{39}$$

To be consistent with Eqs. (22) and (23), a box filter (Eq.(2)) can be used as the smooth function, $G_f^h(\mathbf{x},\mathbf{x}')$. Then the subgrid scale Prandtl number ($\frac{1}{Pr_{SGS}}$) is

$$\frac{1}{Pr_{SGS}} = \frac{1}{C}\frac{\overline{\overline{P}_j\overline{R}_j}}{\overline{\overline{P}_j\overline{P}_j}} \qquad \text{(with the grid filter)} \tag{40}$$

or

$$\frac{1}{Pr_{SGS}} = \frac{1}{C}\frac{\tilde{\overline{P}}_j\overline{R}_j}{\tilde{\overline{P}}_j\overline{P}_j} \qquad \text{(with the test filter)} \tag{41}$$

NUMERICAL PROCEDURE

This study uses a finite difference method to solve the spatially filtered Navier-Stokes equations. It also uses a staggered mesh with a pressure-smoothing technique. All the spatial terms are discretized with the second-order accuracy of the central differencing scheme. A second-order explicit differencing scheme (Explicit Adams-Bashforth Scheme) is used to discretize time. For example, the intermediate velocity, $\overline{u}_i^*$, is calculated by

$$\frac{\overline{u}_i^* - \overline{u}_i^n}{\Delta t} = \frac{3}{2}\left\{ -\frac{1}{\rho}\frac{\partial \overline{P}}{\partial x_i} - \frac{\partial}{\partial x_j}(\overline{u_i}\cdot\overline{u_j}) + \upsilon\frac{\partial^2 \overline{u}_i}{\partial x_i \partial x_j} - \frac{\partial \tau_{ij}}{\partial x_j} + g_j \beta(\overline{\theta} - \theta_0)\delta_{ij} \right\}^n$$
$$-\frac{1}{2}\left\{ -\frac{1}{\rho}\frac{\partial \overline{P}}{\partial x_i} - \frac{\partial}{\partial x_j}(\overline{u_i}\cdot\overline{u_j}) + \upsilon\frac{\partial^2 \overline{u}_i}{\partial x_i \partial x_j} - \frac{\partial \tau_{ij}}{\partial x_j} + g_j \beta(\overline{\theta} - \theta_0)\delta_{ij} \right\}^{n-1} \quad (42)$$

where n is time step and n+1 is the next time step.

By applying a simplified maker and cell (SMAC) method [7], while considering a scalar potential φ which is defined by $\frac{\partial \varphi}{\partial x_i} = u'$, (where $u' = \overline{u}^{n+1} - \overline{u}^*$), and using the continually equation, the scalar potential φ can be written as a Poisson equation

$$\frac{\partial^2 \varphi}{\partial x_i \partial x_i} = -\frac{\partial u_i^*}{\partial x_i} \quad (43)$$

This Poisson equation of the scalar potential φ can be solved by the strong-implicit procedure (SIP) [14]. The final pressure and velocity fields are derived from the auxiliary scalar potential φ though the relations

$$\overline{u}_i^{n+1} = \overline{u}_i^n + \frac{\partial \varphi}{\partial x_i} \quad (44)$$

$$P^{n+1} = P^n - \frac{1}{\Delta t}\varphi \quad (45)$$

APPLICATIONS TO INDOOR AIRFLOW

The FDSM is used to calculate two typical airflows in rooms

- ☞ natural convection in a room with a heated wall and a cooled wall
- ☞ mixed convection in a room with a heated floor and a cold air jet near the ceiling

Natural Convection

The investigation has studied the natural convection flow in a cavity as shown in Fig. 1(a). Cheesewright [2] measured the air velocity, temperature, turbulence energy, and heat transfer in the cavity. The flow characteristics of the cavity are similar to those in a room. The simple geometry eliminates many potential errors, such as those caused by the complex geometry of a baseboard heater. If there are discrepancies between the computed results and measured data, this would allow us to identify the reasons.

Since natural convection consists of both turbulent and laminar flows, it is very challenging to use the LES to simulate the flows. This case enables us to use the DSM, which can be averaged over the depth direction. The depth direction can be considered homogeneous. The LES with the DSM and FDSM ($FDSM_G$ and $FDSM_T$) is used to predict the distributions of air velocity, temperature, and turbulence energy.

Fig. 1(a) shows the cavity geometry (height AC = 2.5 m, width AB = 0.5 m, depth = 0.5 m) as well as the numerical grid distribution used in the LES simulations. The

temperature difference between the warm and cold walls, $\Delta\theta$, is 45.8 K (the left wall temperature, T_1, is 68.0°C, and the right wall temperature, T_2, is 22.2°C). All of the other walls were insulated. The flow corresponds to a Rayleigh number (Ra) of $5.0\text{x}10^{10}$, similar to that found in a typical room. The Ra is defined as

$$\text{Ra} = \frac{(T_1 - T_2)\,gH^3}{\upsilon\alpha} \tag{46}$$

The computations used no-slip velocity conditions for all the walls. The mesh employed was $62 \times 62 \times 12$ for the height (x), width (y), and depth (z) directions, respectively (as shown in Fig. 1(a)). The time step was $\Delta t = 0.0002$ s.

The initial air velocity was zero, and the air temperature was 45.1°C for the whole flow domain. When the flow became statistically steady, the averaging technique was used to obtain the mean value of the computed parameters, such as air velocity and temperature. The averaging time is about 120 s.

Figs. 1(b) and 1(c) show respectively the distributions of average air velocity and temperature with the FDSM_G on the center section (depth = 0.25 m). The velocity field is asymmetric. The hot wall generates an upward flow near the wall and the cold wall a downward flow. The velocity in the center of the cavity is generally small. The flow is laminar in the lower part of the hot wall and the upper part of the cold wall.

Fig. 2 compares the predicted and measured results in the span-wise of the cavity. The results with the DSM (averaging in the depth direction), the FDSM_G, and the FDSM_T agree rather well with the experimental data except near the wall regions. However, the FDSM_G and FDSM_T can predict flow without averaging along a homogeneous direction. This is very important because there is no homogeneous direction in most rooms with natural convection.

As reported by Cheesewright [2], the top and bottom walls of the cavity were not very well insulated. The heat loss in the laboratory environment led to a lower mean air temperature in the cavity. As a result, the predicted mean air temperature in the cavity is higher than the measured data, as illustrated in Fig. 2(b). All models predicted a reasonably good temperature profile.

The present investigation calculates the turbulence energy as $k = (u'^2 + v'^2 + w'^2)/2$ (grid scale). Fig. 2(c) compares the computed k profiles with the experimental data. The DSM model under-predicted the turbulence energy near the walls. The performances of the FDSM_G and FDSM_T are similar to that of the DSM, although they still under-predict the turbulence energy, especially near the walls. The reason may be attributed to the *ad hoc* fix for the coefficient C ($C \geq 0.0$).

This case shows that the FDSM_G and FDSM_T have the same performance as the DSM. Since the FDSM_G and FDSM_T do not need averaging over a homogeneous direction, they can be used to calculate more complex airflow. When comparing the FDSM_G and the FDSM_T, the FDSM_G is slightly better than the FDSM_T.

Mixed Convection

The present investigation also applied the FDSM for mixed convection flow in a room, as shown in Fig. 3(a). Blay et al. [1] measured the air velocity, temperature, and turbulent energy distributions for the case. The geometry of the test rig was H = 1.04 m, L = 1.04 m, and D = 0.7 m. This is a scale-model of a room and has a homogeneous direction (the depth direction) so that the DSM can also be used. The inlet height, h_{in}, was 0.018 m, the supply air velocity, U_{in}, was 0.57 m/s, and the supply air temperature, T_{in}, was 15°C. The outlet height was 0.024m. The test rig used a floor heating system with a floor temperature, T_f, of 35°C. All other wall temperatures, T_w, were 15°C. The corresponding Archimedes

number ($Ar = \frac{\beta g h_{in} \Delta T}{U_{in}^2}$) was 0.0036, and the Reynolds number ($Re = \frac{U_{in} h_{in}}{\nu}$) was 678.

The computations used a non-slip velocity condition for all the walls. The meshes employed were $62 \times 62 \times 12$ for the height (x), width (y), and depth (z) directions.

Figs. 3(b) and 3(c) show the measured mean air velocity distribution and the averaged air velocity distribution using the $FDSM_G$. The measured and computed airflow patterns are almost the same. The LES simulation shows a small re-circulation in the left-bottom corner, but not in the experiment. It is not clear if this is due to insufficient fine measuring points or due to the numerical model used.

Figs. 4 and 5 compare further the predicted mean air velocity, temperature, and turbulent energy distributions using the DSM, $FDSM_G$, and $FDSM_T$ with the experimental data at two center sections (at x = 0.502 m and y = 0.502 m). Figs. 4(a) and 5 (a) show that the three subgrid scale models give very similar air velocity profiles. The $FDSM_G$ performed slightly better than the others. The predicted velocity profiles agree reasonably well with the experimental data.

However, Figs. 4(b) and 5(b) indicate that the predicted air temperature using the three models is about 1.5 K higher than the measured one, though the shape of the predicted temperature profiles is the same as the measured one. The models may overpredict the heat transfer from the floor or underpredict the heat transfer to the other walls. Since no detailed measurements on the heat transfer were available, it is difficult to identify the actual cause of the discrepancies. Perhaps the subgrid scale Prandtl number was not correctly modeled for the buoyancy effect.

Fig. 4(c) illustrates the computed turbulent energy ($k^{1/2} = \{(u'^2+v'^2+w'^2)/2\}^{1/2}$) profiles at section x = 0.502 m and the comparison with the corresponding experimental data. The $FDSM_G$ and DSM can predict the turbulence energy distribution well, while the performance of the $FDSM_T$ was poor. At section y = 0.502 m, all three models overpredicted the turbulence energy, as shown in Fig. 5(c).

The reason for developing the new SGS model is to calculate an indoor airflow without a homogeneous flow direction. However, we have not found suitable experimental or direct-numerical-simulation data for this type of flow from the literature, although the flow exists in most rooms. Validation of the model needs detailed information of Reynolds stresses and heat fluxes. Further research in the direction is needed.

CONCLUSION

This study has developed two filtered dynamic subgrid-scale models (FDSM), one having the grid filter and the other the test filter, for large eddy simulation of complex flow without a homogeneous direction.

The models have been used to predict natural and mixed convection flow in a room. The computed results are compared with the experimental data available from the literature and those with a dynamic subgrid scale model. The FDSM can correctly predict the average air velocity and temperature distributions in a room without a homogenous direction. However, it is more difficult to calculate the heat transfer near a wall and the turbulence energy distribution in a room. The performance of the FDSM is the same as that of the dynamic subgrid scale model, but it can be used for inhomogeneous flows, such as an airflow in a room.

ACKNOWLEDGMENT

The research was supported by the Center for Indoor Air Research, MD.

REFERENCES

1. D. Blay, S. Mergui, and C. Niculae, Confined turbulent mixed convection in the presence of a horizontal buoyant wall jet, *Fundamentals of Mixed Convection*, *ASME HTD-Vol. 213,* pp. 65-72, 1992.
2. R. Cheesewright, K.J. King, and S. Ziai, Experimental data for the validation of computer codes for the prediction of two-dimensional buoyant cavity flows, *ASME Winter Annual Meeting*, *HTD-60,* p.75, Anaheim,1986.
3. L. Davidson and P.V. Nielsen, Large eddy simulation of the flow in a three-dimensional ventilated room, *Preceding of 5th International Conference on Air Distribution in Rooms, ROOMVENT'96*, pp. 161-168, 1996.
4. S. J. Emmerich, and K.B. McGrattan, Application of a large eddy simulation model to study room airflow, *ASHRAE Transactions*, vol. 104, 1998.
5. M. Germano, U. Piomelli, P. Moin, and W.H. Cabot, A dynamic subgrid-scale eddy viscosity model, *J. Physics Fluids* A, vol. 3, p. 1760, 1991.
6. S. Ghosal, T. Lund, P. Moin, and K. Akselvoll, A dynamic localization model for large-eddy simulation of turbulent flows, *J. Fluid Mechanics,* vol. 286, p. 229, 1995.
7. F.H. Harlow and J.E. Welch, Numerical calculation of time-dependent viscous incompressible flow, *J. Physics Fluids,* vol. 8, p. 12, 1965.
8. D.K. Lilly, A proposed modification of the Germano subgrid-scale closure method, *J. Physics Fluids* A, vol. 4, p. 633, 1992.
9. C. Meneveau, T. Lund, and W. Cabot, A Lagrangian dynamic sub-grid scale model of turbulence," *J. Fluid Mechanics*, vol. 315, p. 353 1996.
10. S. Murakami, A. Mochida, and K. Matsui, Large eddy simulation of non-isothermal room airflow, -comparison between standard and dynamic type of Smagorinsky model-, *Journal of Institute of Industrial Science*, University of Tokyo, vol. 47(2), pp. 7-12, 1995.
11. P. Moin, Numerical and physiscal issues in large eddy simulation of turbulent flows, *JSME International Journal* B, vol. 41(2), p. 454, 1998.
12. U. Piomelli, W.H. Cabot, P. Moin, and S. Lee, Subgrid-scale backscatter in turbulent & transitional flows, *J. Physics Fluids* A, vol. 3, p. 1766, 1991.
13. J. Smagorinsky, General circulation experiments with the primitive equations, I: The basic experiment, *Monthly Weather Rev.,* vol. 91, pp. 99-164, 1963.
14. H. L. Stone, Interactive solution of implicit approximations of multidimensional partial differential equations, *SIAM J. of Num. Anal.*, vol. 5, p. 530, 1968.
15. Y. Zang, , R. L. Street, and J. R. Koseff, A dynamic mixed subgrid-scale model and its application to recalculating flow, *J. Physics Fluids* A, vol. 5, p. 3186, 1993.

FIGURE CAPTIONS

Fig. 1 The predicted results of the natural convection in a cavity with the $FDSM_G$ at depth =0.25 m.(a) the cavity geometry, (b) average air velocity, (c) average air temperature.

Fig. 2 Comparison of the predicted and measured results at mid height of the cavity. (a) average air velocity, (b) average air temperature, (c) average turbulent energy.

Fig. 3 The predicted and measured mixed convection flow in a room. (a) room geometry, (b) average velocity vectors obtained from the experiment (Baly et al,1992), (c) average velocity vectors computed by the $FDSM_G$

Fig. 4 Comparison of the predicted and measured results on the center sections (x=0.502m). (a) average velocity, (b) average temperature, (c) average turbulent energy ($k^{1/2}$).

Fig. 5 Comparison of the predicted and measured results on the center sections (y=0.502m). (a) average velocity, (b) average temperature, (c) average turbulent energy ($k^{1/2}$).

To Editor:
Please do not use these scanned images. The quality is not good. Please use the hardcopy instead. Thanks.

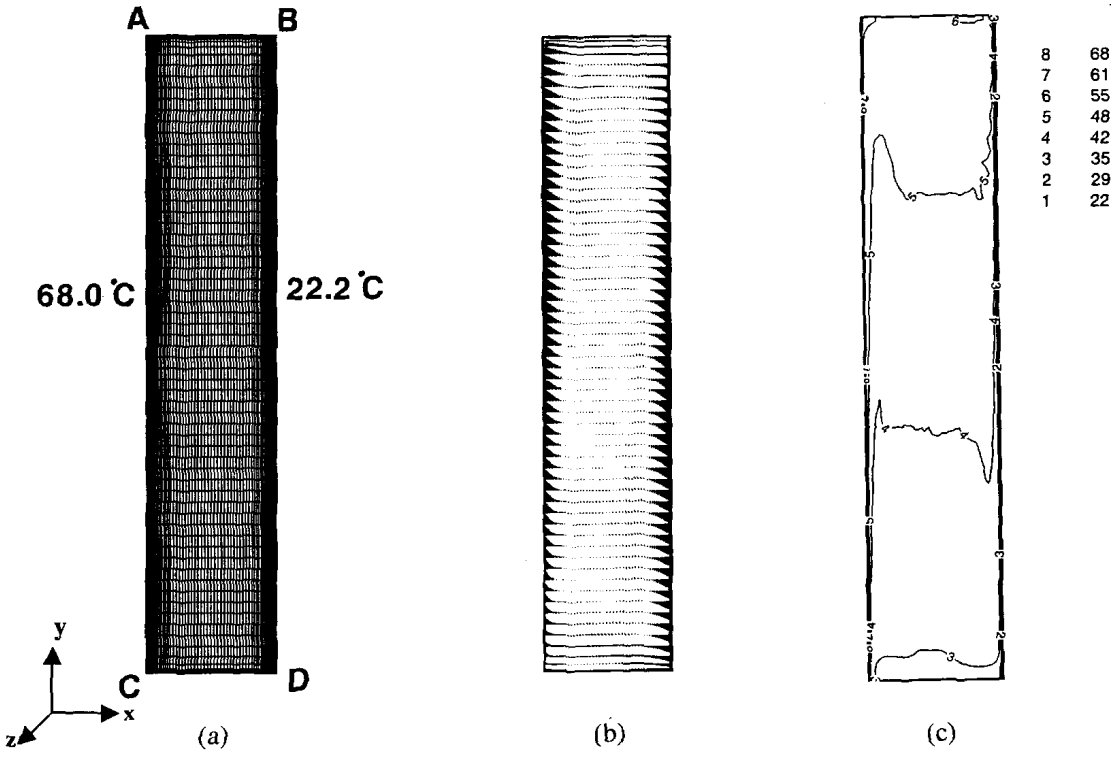

Fig. 1 The predicted results of the natural convection in a cavity with the $FDSM_G$ at depth =0.25 m.
(a) The cavity geometry, (b) average air velocity, (c) average air temperature.

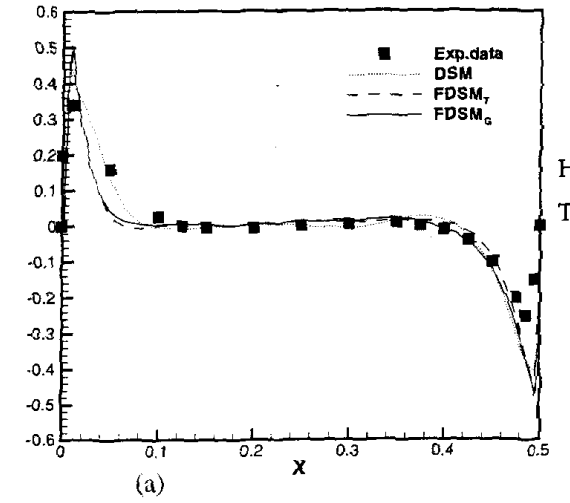

(a)

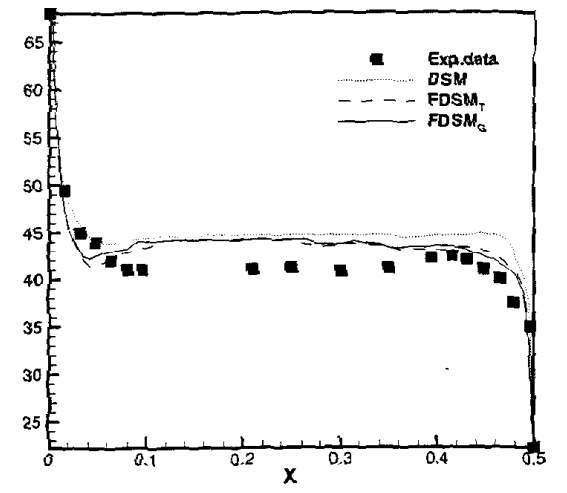

(b)

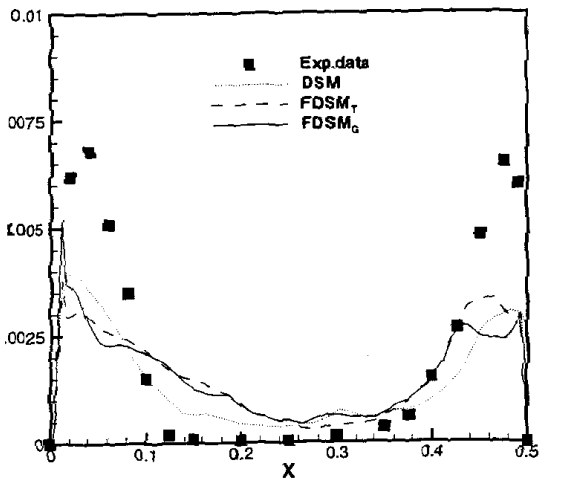

(c)

Fig. 2 Comparison of the predicted and measured results at mid height of the cavity. (a) average air velocity, (b) average air temperature, (c) average turbulent energy.

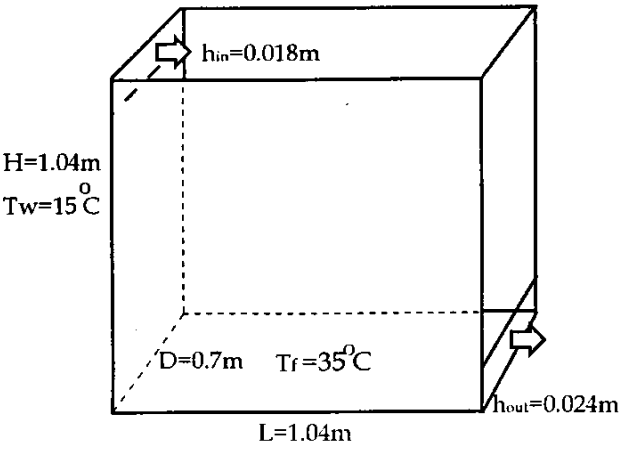

(a)

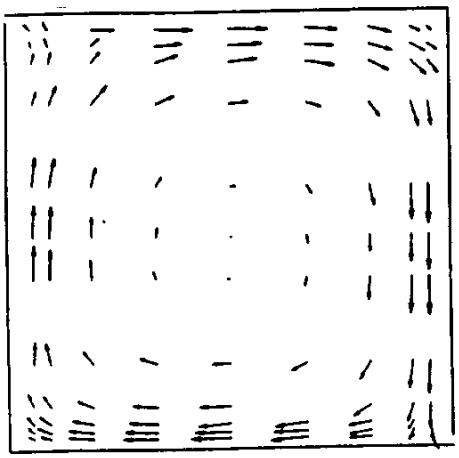

(b)

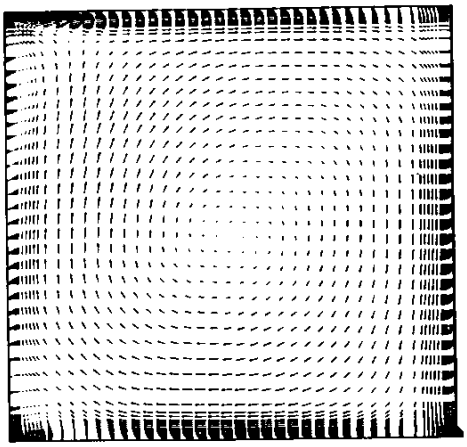

(c)

Fig. 3 The predicted and measured mixed convection flow in a room. (a) room geometry, (b) average velocity vectors obtained from the experiment (Baly et al,1992), (c) average velocity vectors computed by the FDSM$_G$

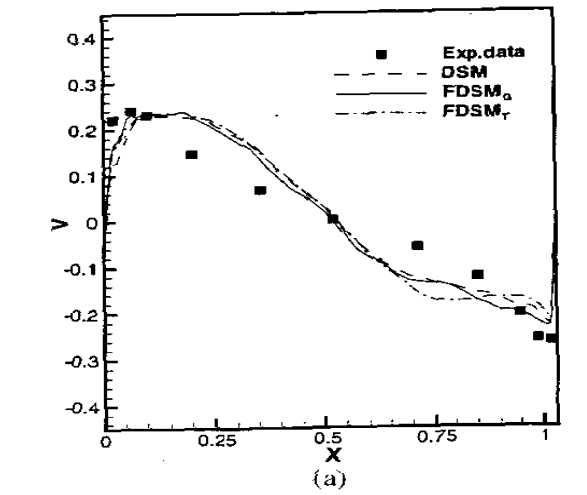

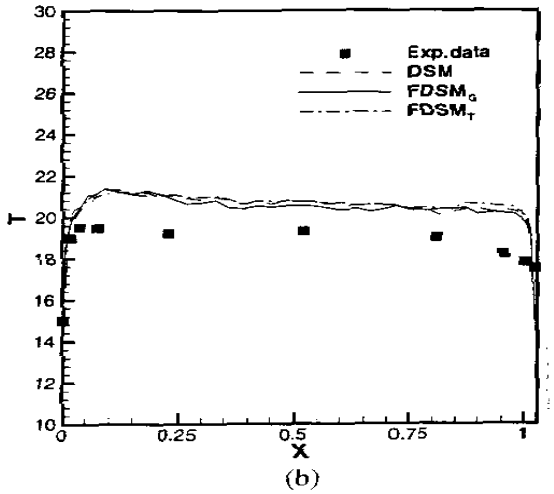

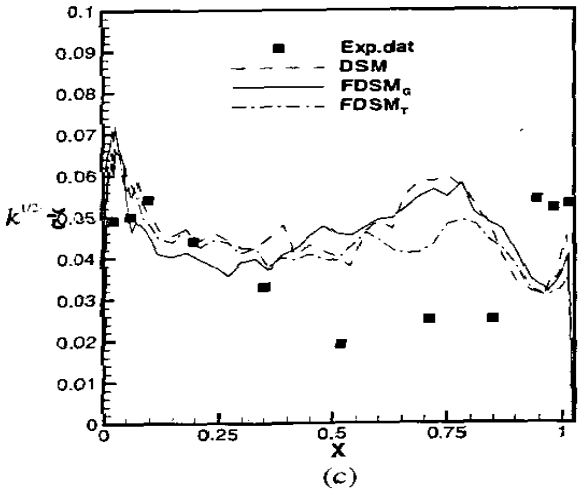

Fig. 4 Comparison of the predicted and measured results on the center sections (X=0.502m). (a) average velocity, (b) average temperature, (c) average turbulent energy ($k^{1/2}$).

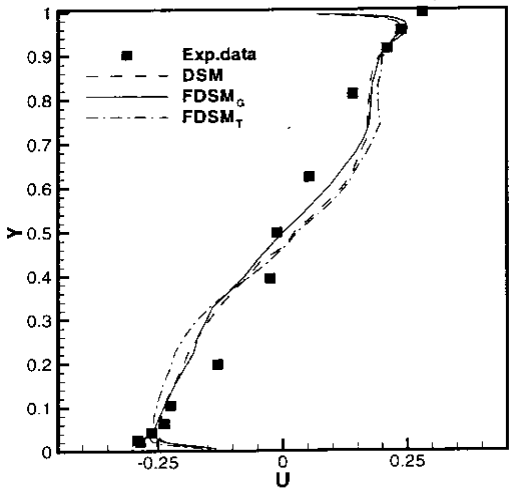

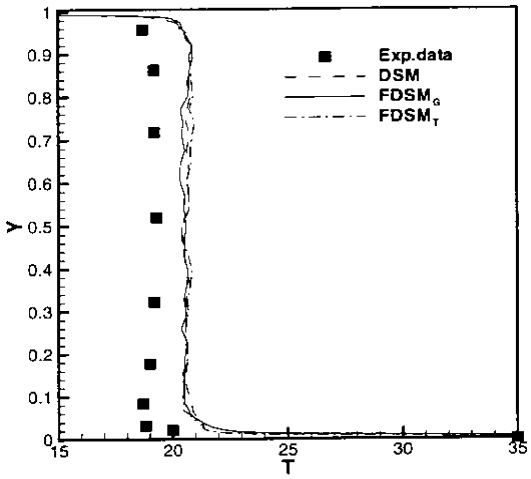

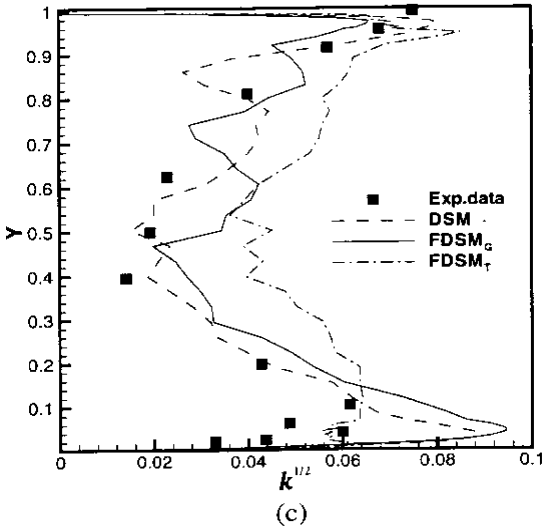

Fig. 5 Comparison of the predicted and measured results on the center sections (Y=0.502m). (a) average velocity, (b) average temperature, (c) average turbulent energy ($k^{1/2}$).